ARTICLE OPEN

Check for updates

Nonreciprocal directional dichroism at telecom wavelengths

K. Park[1], M. O. Yokosuk[1], M. Goryca[2], J. J. Yang[3], S. A. Crooker [2], S. -W. Cheong [4], K. Haule [4], D. Vanderbilt [4], H. -S. Kim [5 ✉] and J. L. Musfeldt [1,6 ✉]

Magnetoelectrics with ultra-low symmetry and spin-orbit coupling are well known to display a number of remarkable properties including nonreciprocal directional dichroism. As a polar and chiral magnet, Ni_3TeO_6 is predicted to host this effect in three fundamentally different configurations, although only two have been experimentally verified. Inspired by the opportunity to unravel the structure-property relations of such a unique light-matter interaction, we combined magneto-optical spectroscopy and first-principles calculations to reveal nonreciprocity in the toroidal geometry and compared our findings with the chiral configurations. We find that formation of Ni toroidal moments is responsible for the largest effects near 1.1 eV—a tendency that is captured by our microscopic model and computational implementation. At the same time, we demonstrate deterministic control of nonreciprocal directional dichroism in Ni_3TeO_6 across the entire telecom wavelength range. This discovery will accelerate the development of photonics applications that take advantage of unusual symmetry characteristics.

INTRODUCTION

The combination of strong spin-orbit coupling and ultra-low symmetry gives rise to many unique properties in materials. One of the most curious is nonreciprocal directional dichroism or 'one-way transparency'[1,2]. Spectroscopically, the effect occurs near a magnetoelectric excitation, often in the THz[3–13] but sometimes extending to the optical region and beyond[14–20], and it arises from the fact that counter-propagating beams can have different absorption coefficients[1,2,21–23]. In other words, a sample may be highly transmitting when measured with light in the $+\mathbf{k}$ direction but nearly opaque in the $-\mathbf{k}$ direction. Nonreciprocity has a number of symmetry prerequisites[22,23]. For a given light propagation direction $\mathbf{k}$, all symmetries that reverse $+\mathbf{k}$ to $-\mathbf{k}$ while leaving the sample unchanged must be broken including inversion, mirrors, and C_2 rotations about a plane or axis perpendicular to $\mathbf{k}$, and time-reversal[21]. Several measurement configurations can be used to take advantage of various types of symmetry breaking[22,23]. Toroidal dichroism occurs when light propagation is along the toroidal moment $\mathbf{T}$ (that is, $\mathbf{k} \parallel \mathbf{T}$), where $\mathbf{T} = \mathbf{P} \times \mathbf{M}$ is the cross product of the electric polarization $\mathbf{P}$ and magnetic moment $\mathbf{M}$[5,9,10,24–26]. Magnetochiral dichroism, on the other hand, involves both chirality and applied magnetic field[8,15,16,27–33]. Interestingly, nonreciprocity can be realized by reversing the external magnetic field as well as the light propagation direction. Linearly- and circularly-polarized light offer additional degrees of freedom[10], and with a vortex beam, one can even select specific projections of the orbital angular momentum[12,13]. The spectroscopic response of these eigenstates is not always equal and opposite, leading to the phenomenon of nonreciprocal directional anisotropy. As a result, unpolarized light can reveal these effects as well[6,16,20].

Because nonreciprocal directional dichroism requires cross-coupling between electric and magnetic dipole transitions, magnetoelectric multiferroics—with their low crystallographic and magnetic symmetries—are promising platforms with which to search for these effects[1,20]. Ni_3TeO_6 is a prominent example. In addition to the natural magnetoelectric character in the vicinity of the antiferromagnetic resonance[12,13], the crystal field (or color band) excitations are magnetoelectric and support broadband nonreciprocal directional dichroism[20]. As a polar + chiral magnet, Ni_3TeO_6 has the potential to host nonreciprocal effects not just in the chiral configurations— which were explored in our prior work[20]—but also in the toroidal geometry. Here, we focus on magneto-optical spectroscopy and first-principles-based simulations of nonreciprocity in the toroidal configuration in order to complete this fascinating series and, at the same time, unravel the structure-property relationships relevant to this unique light-matter interaction. We find that the largest contrast is supported by the $^3A_{2g} \rightarrow {}^3T_{2g}$ on-site excitations near 1.1 eV due to the creation of Ni^{2+} toroidal moments in this relatively narrow energy range—quite different from the magnetochiral and transverse magnetochiral mechanisms that provide broader but more modest effects over the color band range. The phonon side bands that ride on top of these d-to-d excitations are quantitatively assigned to particular phonon modes and shown to display nonreciprocal effects as well. In a significant conceptual advance, we demonstrate dichroic contrast across the telecom range (i.e., optical fiber communication wavelengths). Remarkably, the telecom wavelength range dovetails perfectly with the strongest nonreciprocal response of Ni_3TeO_6 in the toroidal geometry. This establishes a potentially significant application for nonreciprocal materials—beyond ferrites and the microwave regime—in which optical circulators or directional amplifiers can operate in the telecom range with low loss and without complicated sample fabrication[34–37]. These findings also open the door to the use of toroidal magnetoelectrics for optical signal processing and communication[38].

[1]Department of Chemistry, University of Tennessee, Knoxville, TN 37996, USA. [2]National High Magnetic Field Laboratory, Los Alamos, NM 87545, USA. [3]Department of Physics, New Jersey Institute of Technology, Newark, NJ 07102, USA. [4]Department of Physics and Astronomy and Rutgers Center for Emergent Materials, Rutgers University, Piscataway, NJ 08854, USA. [5]Department of Physics and Institute of Quantum Convergence Technology, Kangwon National University, Chuncheon 24341, Korea. [6]Department of Physics and Astronomy, University of Tennessee, Knoxville, TN 37996, USA. ✉email: heungsikim@kangwon.ac.kr; musfeldt@utk.edu

RESULTS AND DISCUSSION

Crystal structure, properties, and symmetry analysis

The crystal structure of Ni_3TeO_6 is both polar and chiral as expected for an $R3$ space group[39]. Chains of distorted NiO_6 and TeO_6 octahedra lie along the c direction, and the three different Ni centers are distinguished by their local environments[40]. In this work, we denote the threefold axis of Ni_3TeO_6 as the 'chiral axis' of the compound[40,41]. Although Ni_3TeO_6 hosts interlocking ferroelectric and chiral domain patterns[40,42], crystals can be polished to reveal a single chiral domain[20]. Below $T_N = 53$ K, the system displays a collinear antiferromagnetic ground state. For $\mathbf{H} \parallel c$, there is a spin-flop transition at 9 T leading to a conical spin and a metamagnetic transition at 52 T—both of which are accompanied by magnetoelastic effects[43–46]. There are no magnetically driven phase transitions when the field is applied perpendicular to the c-axis[44]. The optical properties of Ni_3TeO_6 consist of several different color bands comprised of on-site Ni^{2+} d-to-d excitations along with a charge gap near 2.6 eV[47]. These features are sensitive to the spin-flop and metamagnetic transitions, and because spin-orbit coupling endows the excitations with magnetoelectric character, these phases support nonreciprocal directional dichroism[20]. Here, the excited Ni state (with a hole in the t_{2g} orbital) provides spin-orbit coupling on the order of 40 meV and assures that the matrix elements containing polarization and magnetization are non-zero[20]. Significantly, the broadband nonreciprocal directional dichroism in the magnetochiral configuration of Ni_3TeO_6 can be modeled using a quantitative first-principles-derived formalism[20].

Figure 1 summarizes our overall approach and the symmetry conditions that are important in this work. We begin by calculating absorption difference spectra as $\Delta\alpha = \alpha(\mathbf{H}) - \alpha(0 \text{ T})$ for the different measurement configurations. Nonreciprocity is determined from various differences in the $\Delta\alpha$ spectra, for instance $\Delta\alpha_{NDD}(+\mathbf{k}, \pm\mathbf{H}) = \Delta\alpha(+\mathbf{k}, +\mathbf{H}) - \Delta\alpha(+\mathbf{k}, -\mathbf{H})$ (Fig. 1a). Notice that when both $\mathbf{k}$ and $\mathbf{H}$ are reversed, $\alpha_{NDD}(\pm\mathbf{k}, \pm\mathbf{H}) = \Delta\alpha(+\mathbf{k}, +\mathbf{H}) - \Delta\alpha(-\mathbf{k}, -\mathbf{H})$ vanishes (Fig. 1b). Nonreciprocity can also be defined in terms of counter-propagating beams, $\Delta\alpha_{NDD}(\pm\mathbf{k}, +\mathbf{H})$, as shown in Fig. 2.

The top panels in Fig. 2 summarize the three different measurement configurations predicted within the framework of symmetry operational similarity[22,23]. In the toroidal configuration

(Fig. 2a), electric polarization along c, combined with $\mathbf{H}$ perpendicular to c, breaks twofold rotation, inversion, mirror, and time-reversal symmetries, so it has symmetry operational similarity with the wave vector of light $\mathbf{k}$ along the third direction. Thus, light propagation parallel to the toroidal moment can exhibit nonreciprocal directional dichroism. The two other configurations of interest involve chirality (rather than electric polarization) which breaks inversion and mirror symmetries. The magnetochiral geometry is obtained when the light propagation direction and applied field are parallel to the chiral axis (Fig. 2b). The transverse magnetochiral configuration, on the other hand, requires both the light propagation direction and magnetic field to be perpendicular to the chiral axis (Fig. 2c). Note that we denote the C_3 axis in Ni_3TeO_6 as the chiral axis; previous studies have argued that nonreciprocity in chiral systems can be easily understood considering chirality as a vector-like quantity[22,41].

Nonreciprocal effect in different measurement configurations

Figure 2 summarizes nonreciprocal directional dichroism of Ni_3TeO_6 at full field in the toroidal, magnetochiral, and transverse magnetochiral configurations. Overall, this behavior is a consequence of low symmetry, structural and magnetic chirality, and the presence of spin-orbit coupling, although the specific appearance of $\Delta\alpha_{NDD}$ depends upon the measurement configuration as well. Focusing first on Ni_3TeO_6 in the toroidal geometry (Fig. 2a), we find a strong dichroic response in the vicinity of the 1.1 eV color band. This feature is assigned as a superposition of Ni^{2+} on-site d-to-d excitations ($^3A_{2g} \rightarrow {}^3T_{2g}$) emanating from the three different local environments of the Ni centers[47]. At 60 T, the largest field-induced changes are centered on the 1.1 eV color band and are on the order of 160 cm^{-1}. This corresponds to between zero and ~45% contrast, depending on the value of the absolute absorption. The dichroic contrast in the vicinity of the $^3A_{2g} \rightarrow {}^1E_g$ and $^3A_{2g} \rightarrow {}^3T_{1g}$ color bands is significantly smaller, and that at higher energy near the $^3A_g \rightarrow {}^1T_{2g}$ excitation is zero within our sensitivity. In the toroidal configuration, the overall size of $\Delta\alpha_{NDD}$ and its energy distribution is quite different than what is observed in the magnetochiral and transverse magnetochiral geometries[20]. For instance, while all configurations exhibit
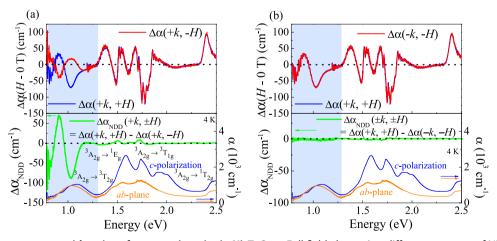

Fig. 1 Illustrating symmetry considerations for nonreciprocity in Ni_3TeO_6. a Full field absorption difference spectra of Ni_3TeO_6 as a function of energy for the $(+\mathbf{k}, +\mathbf{H})$ and $(+\mathbf{k}, -\mathbf{H})$ configurations in the toroidal measurement geometry. For illustration purposes, we employ $\mathbf{H} = 60$ T. Nonreciprocal directional dichroism is shown in green. Here, $\Delta\alpha_{NDD}(+\mathbf{k}, \pm\mathbf{H}) = \Delta\alpha(+\mathbf{k}, +\mathbf{H}) - \Delta\alpha(+\mathbf{k}, -\mathbf{H})$. Experimentally, it is common to reverse the magnetic field direction as we have done here. Nonreciprocity can also be defined in terms of counter-propagating beams, $\Delta\alpha_{NDD}(\pm\mathbf{k}, +\mathbf{H})$, as shown in Fig. 2. **b** Full field absorption difference spectra in the $(+\mathbf{k}, +\mathbf{H})$ and $(-\mathbf{k}, -\mathbf{H})$ configurations. Notice that they are the same. $\alpha_{NDD}(\pm\mathbf{k}, \pm\mathbf{H}) = \Delta\alpha(+\mathbf{k}, +\mathbf{H}) - \Delta\alpha(-\mathbf{k}, -\mathbf{H})$ (also shown in green) vanishes when both light propagation and magnetic field direction are switched simultaneously. The absolute absorption spectrum is shown at the bottom of each panel to provide context. Note that we used cubic term symbols here ($^3A_{2g}$, $^3T_{2g}$, ^1E_g, $^3T_{1g}$, $^1T_{2g}$) to denote Ni^{2+} atomic multiplets because the deviation from cubic symmetry by trigonal distortion at the Ni sites is small (≈ 0.1 eV in terms of crystal fields).
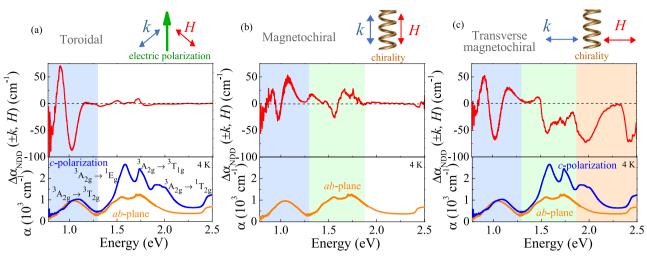
Fig. 2 Nonreciprocity of Ni₃TeO₆ in the three different measurement configurations. Summary of the three different measurement configurations of interest in this work: **a** toroidal (**k** ⊥ **H** ⊥ polarization, **b** magnetochiral (**k** ∥ **H** ∥ chirality), and **c** transverse magnetochiral (**k** ∥ **H** ⊥ chirality). Nonreciprocal directional dichroism spectra of Ni₃TeO₆ at 60 T in the toroidal (**a**), magnetochiral (**b**), and transverse magnetochiral (**c**) configurations, respectively. These spectra were measured in the Voigt (**a**) and Faraday (**b**, **c**) geometries. The nonreciprocal responses in panels (**b**, **c**) are reproduced from ref. [20]. The linear absorption spectrum of Ni₃TeO₆ at 4.2 K is shown below each nonreciprocal panel for comparison. The polarization directions and on-site Ni d-to-d excitations are labeled.

dichroic contrast near the 1.1 eV color band, that in the toroidal configuration is by far the largest.

Turning to nonreciprocal directional dichroism of Ni₃TeO₆ in the magnetochiral configuration (Fig. 2b), $\Delta\alpha_{NDD}$ associated with the 1.1 and 1.65 eV color bands is on the order of ±45 cm⁻¹ at full field[20]. This is different than what we find in the toroidal configuration both in terms of size and shape. There is a lot more fine structure to $\Delta\alpha_{NDD}$ in the magnetochiral configuration as well. Unlike the other two measurement configurations shown in Fig. 2, $\Delta\alpha_{NDD}$ in the magnetochiral geometry appears only above the 9 T spin flop transition where spin canting introduces net magnetization[43,47]. The nonreciprocal response of Ni₃TeO₆ is different yet again in the transverse magnetochiral configuration with dichroic contrast associated with all four types of d-to-d excitations in the absolute absorption spectrum (Fig. 2c). This suggests that the color bands have magnetoelectric character in the chiral geometries as well. Differences in magnetoelectric coupling as it pertains to the various contrasts in toroidal, magnetochiral, and transverse magnetochiral geometries are discussed below.

Field dependence of the dichroic contrast in the toroidal geometry

Figure 3a displays nonreciprocal directional dichroism of Ni₃TeO₆ as a function of magnetic field in the toroidal configuration. As discussed previously, the toroidal geometry involves placing the electric polarization direction mutually orthogonal to both the light propagation and magnetic field directions. In addition to large positive and negative lobes in the dichroic contrast, there is a great deal of fine structure below 0.9 eV. These features can be assigned to phonon sidebands as discussed below. Examination reveals that α_{NDD} appears at the lowest fields and grows systematically. This is because field-induced canting of Ni moments, which gives rise to net ferromagnetic moments and enables nonreciprocal behavior, can occur even at the smallest fields. That nonreciprocal directional dichroism can be seen at low fields is useful for a number of applications including optical isolators and rectifiers, high-fidelity holograms, and potentially in the telecom sector. In any case, we can quantify this trend by integrating α_{NDD} over an appropriate energy window and plotting the result as a function of the applied field (inset, Fig. 3a).

The shape reveals how the spins align in the direction of the applied field. The lack of sharp jumps or cusps is consistent with the absence of field-induced magnetic transitions for **H** ⊥c[44]. No hysteresis is observed. In addition to switching the applied field direction, we investigated symmetry effects[41] in Ni₃TeO₆ by switching the light propagation direction (Supplementary Fig. 1). The results are identical. If both light propagation and the magnetic field directions are switched at the same time, nonreciprocal directional dichroism vanishes due to time-reversal symmetry (Fig. 1b and Supplementary Fig. 2)[41].

Comparison between the experimental nonreciprocal directional dichroism in different geometries with the simulated versions provides insight into the nature of the contrast in different energy ranges. Figure 3b displays $\Delta\alpha_{NDD}$ of Ni₃TeO₆ calculated by first-principles-based methods in the toroidal configuration[20]. The simulated spectrum compares reasonably well with the experimental result, except for the phonon sideband effects around 0.8 eV which are not included in the model, capturing the maximum near 0.9 eV, the minimum near 1.03 eV as well as the lack of contrast at higher energies. Note that our simulation is based upon a local ionic picture and includes only intra-Ni-ionic excitations[20], not the entire part of the structural (and magnetic) chirality of Ni₃TeO₆. The structural chirality of Ni₃TeO₆ manifests (i) at the local level with a chiral crystal-field environment at each Ni site as well as (ii) in the global arrangement of Ni sites. Our theory includes the former but not the latter. We refer to these as local and global chirality, respectively[48]. Based on the results from our ionic picture-based simulation that nicely capture the dichroic response near 1 eV, we speculate that excitations near 1 eV are relevant to the local chiral component, namely the formation of the Ni ionic toroidal moments perpendicular to the magnetic field and bulk electric polarization (**T** ≡ **P** × **M**), which are coupled with the propagation of light and induce nonreciprocal directional dichroism[41]. On the other hand, nonreciprocity at higher energies, which is sizable only in the magnetochiral and transverse magnetochiral cases (Fig. 2b, c), originates primarily from global chirality and is difficult to capture within our atomistic simulation framework. Since our simulated nonreciprocal directional dichroism is given as a sum of individual Ni atomic contributions, some aspects of global chirality originating from arrangements of Ni sites at different Wyckoff positions may partially cancel out to yield smaller responses
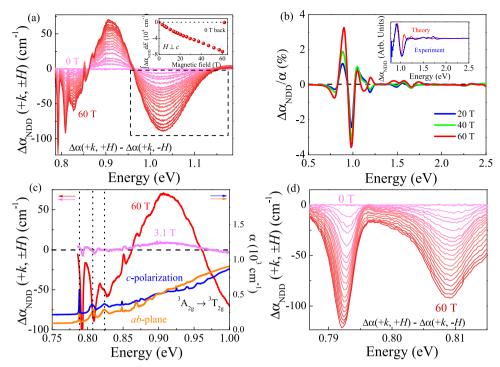
Fig. 3 Nonreciprocity in the toroidal geometry. a Nonreciprocal directional dichroism of Ni_3TeO_6 in the toroidal configuration measured between 0 and 60 T at 4.0 K. The inset is the integration of the indicated feature in the dashed box over an appropriate energy window. No hysteresis is observed. **b** Simulated nonreciprocal directional dichroism of Ni_3TeO_6 in the toroidal configuration. The inset shows a comparison of the calculated and measured results at 60 T. The intensity is normalized to the maximum of $\Delta\alpha_{NDD}$. **c** Close-up view of $\Delta\alpha_{NDD}$ at 3.1 and 60 T compared with the linear absorption spectrum. **d** Close-up view of $\Delta\alpha_{NDD}$ as a function of field between 0 and 60 T. The complete list of magnetic fields in panels (**a**) and (**d**) is: 0, 3.1, 5.5, 7.2, 10.7, 13.8, 15.8, 17.9, 20.3, 23.1, 26.1, 29.6, 33.3, 37.5, 42.1, 47.0, 52.1, 57.1, 60.2 T.

compared to experimental results. Details are available in the Methods section and in Supplementary information (Supplementary Notes 1.3).

Antiferromagnets traditionally offer foundational opportunities to investigate collective excitations that arise from charge-spin and charge-lattice coupling[49]. These features include excitons, zero phonon lines, phonon sidebands, and magnon sidebands. They are commonly observed on the leading edge of the lowest energy d-to-d band in antiferromagnets like MnF_2 and α-Fe_2O_3[50,51]. The absorption spectrum of Ni_3TeO_6 does not have a zero phonon line because it is in the strong coupling limit[52], but it does have a rich set of phonon sidebands on the leading edge of the $^3A_{2g} \rightarrow {}^3T_{2g}$ excitation (Fig. 3c and Supplementary Fig. 6)[20]. These structures, often called 'phonon replicas', arise from vibronic coupling, the details of which are characterized by the Huang-Rhys factor[52,53]. That the phonon progression on the leading edge of the Ni^{2+} d-to-d excitations matches features in $\Delta\alpha_{NDD}$ illustrates the physical connection and demonstrates that the phonon sidebands have a magnetoelectric character. Nonreciprocal directional dichroism thus provides an opportunity to investigate how phonons activated in this manner are impacted by reversing the field and/or light propagation direction. At this time, there are only a handful of cases ($BiFeO_3$, few-layer CrI_3, and Cu_2OSeO_3) where phonons or phonon-derived properties such as thermal conductivity have been shown to host nonreciprocal effects[4,25,54,55]. Nonreciprocal phonons obviously enable rectification of heat and sound[55]— a topic of sustained interest. A giant nonreciprocal response in the THz range has recently been reported in Ni_3TeO_6[11], possibly originating from the effects mentioned above. Below, we demonstrate that the phonon sidebands in Ni_3TeO_6 not only display nonreciprocal directional dichroism (Fig. 3d) but that this contrast occurs along with that related to the low-energy Ni^{2+} crystal field excitations across the telecom range.

Nonreciprocal directional dichroism at telecom wavelengths

We, therefore, return to the spectra in Fig. 3c which are even more intriguing when overlaid with the useful telecom bands. The latter include the O-, E-, S-, C-, L- and U-bands. Optical fiber communications typically operate in one of these windows. The C-band (1530–1565 nm) is perhaps most familiar and employs drawn Er-glass fibers. While the optical properties of Er-glass fibers have been studied separately under electric and magnetic fields[56–60], we are unaware of any attempt to explore rectification effects. Moreover, nonreciprocal directional dichroism has been revealed in a number of different energy regimes, it is rarely encountered in the near infrared[7,29].

Figure 4 displays a close-up view of the nonreciprocal directional dichroism in Ni_3TeO_6 in the toroidal configuration plotted on a percentage basis and a wavelength scale. Examination reveals that $\Delta\alpha_{NDD}$ has a near-perfect match to the full range of telecom wavelengths. The effects are strong, broad, and clearly evident at the full field (60 T) with a maximum contrast in the first phonon sideband of approximately 45%. These features also appear even at the smallest fields (as shown by the spectrum at 3.1 T) because time-reversal is already broken. This, along with the fact that we are using unpolarized light, is an advantage for applications. Difference signals are already in regular use, and nonreciprocal effects can add an important layer of security. Ni_3TeO_6 hosts similar contrast in the magnetochiral and transverse magnetochiral configurations as well (Supplementary Fig. 7). In addition to demonstrating that nonreciprocal directional dichroism can be positioned within useful telecom windows, this work opens the door to the development of high efficiency/low dissipation optical diodes and rectifiers from crystalline materials. We anticipate that linear or circular polarizers would amplify the size of this effect in Ni_3TeO_6, but the ability to achieve a polarization-independent signal is one of the advantages of magnetochiral materials.
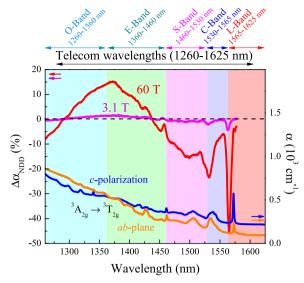
Fig. 4 Nonreciprocity at telecom wavelengths. Close-up view of nonreciprocal directional dichroism in Ni_3TeO_6 on a percentage basis as a function of wavelength in the toroidal configuration at 4.0 K. $\Delta\alpha_{NDD}$ is shown at 3.1 and 60 T. The absolute absorption spectrum is included for comparison. Various commercial telecom windows are summarized on the upper axis. The U-band (1625–1675 nm) is not shown.

Structure-property relations for photonics applications

Ni_3TeO_6 is a superb platform for fundamental studies of nonreciprocity because it hosts this peculiar property across a wide range of excitations and in three different measurement configurations. To our knowledge, there are no other nonreciprocal materials that have been studied in so many different geometries. In this work, we focus on the Ni^{2+} d-to-d excitations and associated phonon sidebands in the near infrared and optical range in the toroidal configuration, unraveling structure-property relationships via comparison with the magnetochiral and transverse magnetochiral geometries. We find that polarity allows the creation of Ni toroidal moments, which results in large contrast near the color band at 1.1 eV. The chiral geometries, on the other hand, yield smaller contrast over a much broader energy range. Our modeling of the size and shape of the spectral response supports this picture of the importance of polarity vs. chirality in the creation of large vs. broadband contrast. These findings enhance our ability to design and deliver complex materials properties on demand. At the same time, the discovery of nonreciprocal effects across the full telecom wavelength range presents a number of exciting opportunities. While tunability under magnetic field is established in this work, the degree to which nonreciprocity can be controlled by other external stimuli or chemical substitution is unexplored. That said, the discovery of nonreciprocity in the telecom region is a significant conceptual advance that has the potential to jump-start the use of dichroic contrast in photonics applications—particularly in the area of high-efficiency optical diodes and rectifiers.

METHODS

Crystal growth and orientation

High-quality single crystals of Ni_3TeO_6 were grown by chemical vapor transport methods as described previously[43]. The crystals were polished to expose either the ab-plane or the c-axis and to control optical density. After polishing, the sample thicknesses were on the order of 30 μm. Optical microscope images and optical rotation data confirm that the crystals have

a single chiral domain[20]. The crystals were coated with transparent epoxy to support and mechanically stabilize the structure during the field pulses.

Optical spectroscopy

Polarized optical transmittance was measured as a function of photon energy E and temperature using a series of spectrometers as described previously (0.78– 2.5 eV; 4.2–300 K)[45]. Absorption was calculated as $\alpha(E) = \frac{1}{d}\ln(T(E))$, where d is the sample thickness and $T(E)$ is the measured transmittance.

Magneto-optical spectroscopy

Magneto-optical work was performed in the toroidal geometry in a capacitor-driven 65 T pulsed magnet at the National High Magnetic Field Laboratory in Los Alamos, NM. We employed the standard transmission probe fitted with a specially designed Voigt end-piece for this work. These measurements covered the 0.75–2.6 eV range with 2.4 meV resolution and were carried out at 4 K. Broadband light from a tungsten lamp was coupled to optical fibers and focused through the sample for transmittance experiments. A collection fiber brought the light from the top of the probe to the grating spectrometer, where both CCD and InGaAs detectors were employed as appropriate. The spectra were taken in four different measurement configurations: (±**k**, ±**H**). Each run was carried out sequentially and consistently, starting with one **k** direction (and pulsing to obtain both ±**H**) and then switching to the other **k** direction by swapping the fibers (again pulsing both up and down). We calculated the absorption differences as: $\Delta\alpha = \alpha(\mathbf{H} = \pm 60\,\text{T}) - \alpha(\mathbf{H} = 0\,\text{T})$. As an example, nonreciprocal directional dichroism is calculated as: $\Delta\alpha_{NDD}(+\mathbf{k}, \pm\mathbf{H}) = \Delta\alpha(+\mathbf{k}, +\mathbf{H}) - \Delta\alpha(+\mathbf{k}, -\mathbf{H})$. Nonreciprocity can also be defined in terms of counter-propagating beams as $\Delta\alpha_{NDD}(\pm\mathbf{k}, +\mathbf{H})$. Traditional smoothing techniques were employed in the CCD detector regime.

Modeling the optical diode effect

Magnetic configurations under the external **H**-field were found by optimizing the total energies of a magnetic exchange Hamiltonian derived from previous first-principles electronic structure calculations[44]. Distortions in the crystal structure induced by the external **H**-field were simulated by enforcing magnetic configurations obtained from the model optimization above during the first-principles density functional theory (DFT) calculations and structural relaxations, which were performed via the Vienna ab-initio Simulation Package (VASP)[61,62]. For VASP structural relaxations we employed a 500 eV of plane-wave energy cutoff, a $5 \times 5 \times 5$ Γ-centered **k**-point sampling, and a simplified rotationally invariant DFT + U_{eff} formalism ($U_{eff} = 4$ eV)[63] on top of PBEsol exchange-correlation functional[64]. After structural relaxations, WIEN2K full-potential DFT code[65] was used to compute electric dipole matrix elements and crystal fields in terms of the non-interacting band basis, which were then projected onto Ni^{2+} atomic multiplet states via exact diagonalization (ED) routine included in the Embedded DMFT Functional (EDMFTF) code[66]. Details on WIEN2K, ED calculations, computations of electric and magnetic dipole matrix elements, and estimations of magneto-electric response tensors are presented in our previous work[20].

REFERENCES

1. Kézsmárki, I. et al. One-way transparency of four-coloured spin-wave excitations in multiferroic materials. *Nat. Commun.* **5**, 3203 (2014).
2. Tokura, Y. & Nagaosa, N. Nonreciprocal responses from non-centrosymmetric quantum materials. *Nat. Commun.* **9**, 3740 (2018).

3. Kézsmárki, I. et al. Optical diode effect at spin-wave excitations of the room-temperature multiferroic BiFeO$_3$. *Phys. Rev. Lett.* **115**, 127203 (2015).

4. Lee, J. H., Kézsmárki, I. & Fishman, R. S. First-principles approach to the dynamic magnetoelectric couplings for the non-reciprocal directional dichroism in BiFeO$_3$. *N. J. Phys.* **18**, 043025 (2016).

5. Bordács, S. et al. Unidirectional terahertz light absorption in the pyroelectric ferrimagnet CaBaCo$_4$O$_7$. *Phys. Rev. B* **92**, 214441 (2015).

6. Yu, S. et al. High-temperature terahertz optical diode effect without magnetic order in polar FeZnMo$_3$O$_8$. *Phys. Rev. Lett.* **120**, 037601 (2018).

7. Sheu, Y. M. et al. Picosecond creation of switchable optomagnets from a polar antiferromagnet with giant photoinduced Kerr rotations. *Phys. Rev. X* **9**, 031038 (2019).

8. Bordács, S. et al. Chirality of matter shows up via spin excitations. *Nat. Phys.* **8**, 734–738 (2012).

9. Kézsmárki, I. et al. Enhanced directional dichroism of terahertz light in resonance with magnetic excitations of the multiferroic Ba$_2$CoGe$_2$O$_7$ oxide compound. *Phys. Rev. Lett.* **106**, 057403 (2011).

10. Narita, H. et al. Observation of nonreciprocal directional dichroism via electro-magnon resonance in a chiral-lattice helimagnet Ba$_3$NbFe$_3$Si$_2$O$_{14}$. *Phys. Rev. B* **94**, 094433 (2016).

11. Langenbach, M. *Giant Directional Dichroism in Chiral Ni$_3$TeO$_6$ in THz Spectroscopy in High Magnetic Fields*. Ph.D. thesis (2019). https://www.semanticscholar.org/paper/Giant-directional-dichroism-in-chiral-Ni_3TeO_6-in-Langenbach/8fda74dc714b6c626d6b9897a958e69aa0e30495.

12. Sirenko, A. A. et al. Terahertz vortex beam as a spectroscopic probe of magnetic excitations. *Phys. Rev. Lett.* **122**, 237401 (2019).

13. Sirenko, A. A. et al. Total angular momentum dichroism of the terahertz vortex beams at the antiferromagnetic resonances. *Phys. Rev. Lett.* **126**, 157401 (2021).

14. Jung, J. H. et al. Optical magnetoelectric effect in the polar GaFeO$_3$ ferrimagnet. *Phys. Rev. Lett.* **93**, 037403 (2004).

15. Saito, M., Taniguchi, K. & Arima, T. Gigantic optical magnetoelectric effect in CuB$_2$O$_4$. *J. Phys. Soc. Jpn* **77**, 013705 (2008).

16. Saito, M., Ishikawa, K., Taniguchi, K. & Arima, T. Magnetic control of crystal chirality and the existence of a large magneto-optical dichroism effect in CuB$_2$O$_4$. *Phys. Rev. Lett.* **101**, 117402 (2008).

17. Toyoda, S. et al. One-way transparency of light in multiferroic CuB$_2$O$_4$. *Phys. Rev. Lett.* **115**, 267207 (2015).

18. Saito, M., Ishikawa, K., Taniguchi, K. & Arima, T. Magnetically controllable CuB$_2$O$_4$ phase retarder. *Appl. Phys. Express* **1**, 121302 (2008).

19. Saito, M., Ishikawa, K., Konno, S., Taniguchi, K. & Arima, T. Periodic rotation of magnetization in a non-centrosymmetric soft magnet induced by an electric field. *Nat. Mater.* **8**, 634–638 (2009).

20. Yokosuk, M. O. et al. Nonreciprocal directional dichroism of a chiral magnet in the visible range. *npj Quant. Mater.* **5**, 20 (2020).

21. Szaller, D., Bordács, S. & Kézsmárki, I. Symmetry conditions for nonreciprocal light propagation in magnetic crystals. *Phys. Rev. B* **87**, 014421 (2013).

22. Cheong, S.-W., Talbayev, D., Kiryukhin, V. & Saxena, A. Broken symmetries, non-reciprocity, and multiferroicity. *npj Quant. Mater.* **3**, 19 (2018).

23. Cheong, S.-W. SOS: symmetry-operational similarity. *npj Quant. Mater.* **4**, 53 (2019).

24. Rikken, G. L. J. A., Strohm, C. & Wyder, P. Observation of magnetoelectric directional anisotropy. *Phys. Rev. Lett.* **89**, 133005 (2002).

25. Fishman, R. S. et al. Spin-induced polarizations and nonreciprocal directional dichroism of the room-temperature multiferroic BiFeO$_3$. *Phys. Rev. B* **92**, 094422 (2015).

26. Ding, L. et al. Field-tunable toroidal moment in a chiral-lattice magnet. *Nat. Commun.* **12**, 5339 (2021).

27. Rikken, G. L. J. A. & Raupach, E. Observation of magneto-chiral dichroism. *Nature* **390**, 493–494 (1997).

28. Sessoli, R. et al. Strong magneto-chiral dichroism in a paramagnetic molecular helix observed by hard X-rays. *Nat. Phys.* **11**, 69–74 (2015).

29. Nakagawa, N. et al. Magneto-chiral dichroism of CsCuCl$_3$. *Phys. Rev. B* **96**, 121102 (2017).

30. Train, C., Gruselle, M. & Verdaguer, M. The fruitful introduction of chirality and control of absolute configurations in molecular magnets. *Chem. Soc. Rev.* **40**, 3297 (2011).

31. Barron, L. D. Chirality and magnetism shake hands. *Nat. Mater.* **7**, 691–692 (2008).

32. Train, C. et al. Strong magneto-chiral dichroism in enantiopure chiral ferro-magnets. *Nat. Mater.* **7**, 729–734 (2008).

33. Sakano, M. et al. Radial spin texture in elemental tellurium with chiral crystal structure. *Phys. Rev. Lett.* **124**, 136404 (2020).

34. Bi, L. et al. On-chip optical isolation in monolithically integrated non-reciprocal optical resonators. *Nat. Photon.* **5**, 758–762 (2011).

35. Manipatruni, S., Robinson, J. T. & Lipson, M. Optical nonreciprocity in opto-mechanical structures. *Phys. Rev. Lett.* **102**, 213903 (2009).

36. Peng, B. et al. Parity–time-symmetric whispering-gallery microcavities. *Nat. Phys.* **10**, 394–398 (2014).

37. Scheucher, M., Hilico, A., Will, E., Volz, J. & Rauschenbeutel, A. Quantum optical circulator controlled by a single chirally coupled atom. *Science* **354**, 1577–1580 (2016).

38. Pozar, D. M. *Microwave Engineering* (Wiley, 2011).

39. Živković, I., Prša, K., Zaharko, O. & Berger, H. Ni$_3$TeO$_6$ – a collinear antiferromagnet with ferromagnetic honeycomb planes. *J. Phys.: Condens. Matter* **22**, 056002 (2010).

40. Wang, X., Huang, F.-T., Yang, J., Oh, Y. S. & Cheong, S.-W. Interlocked chiral/polar domain walls and large optical rotation in Ni$_3$TeO$_6$. *APL Mater.* **3**, 076105 (2015).

41. Hlinka, J. Eight types of symmetrically distinct vectorlike physical quantities. *Phys. Rev. Lett.* **113**, 165502 (2014).

42. Ye, M. & Vanderbilt, D. Domain walls and ferroelectric reversal in corundum derivatives. *Phys. Rev. B* **95**, 014105 (2017).

43. Oh, Y. S. et al. Non-hysteretic colossal magnetoelectricity in a collinear anti-ferromagnet. *Nat. Commun.* **5**, 3201 (2014).

44. Kim, J. W. et al. Successive magnetic-field-induced transitions and colossal magnetoelectric effect in Ni$_3$TeO$_6$. *Phys. Rev. Lett.* **115**, 137201 (2015).

45. Yokosuk, M. O. et al. Tracking the continuous spin-flop transition in Ni$_3$TeO$_6$ by infrared spectroscopy. *Phys. Rev. B* **92**, 144305 (2015).

46. Lass, J. et al. Field-induced magnetic incommensurability in multiferroic Ni$_3$TeO$_6$. *Phys. Rev. B* **101**, 054415 (2020).

47. Yokosuk, M. O. et al. Magnetoelectric coupling through the spin flop transition in Ni$_3$TeO$_6$. *Phys. Rev. Lett.* **117**, 147402 (2016).

48. Zhou, X., Feng, W., Yang, X., Guo, G.-Y. & Yao, Y. Crystal chirality magneto-optical effects in collinear antiferromagnets. *Phys. Rev. B* **104**, 024401 (2021).

49. Sell, D. D., Greene, R. L. & White, R. M. Optical exciton-magnon absorption in MnF$_2$. *Phys. Rev.* **158**, 489–510 (1967).

50. Greene, R. L., Sell, D. D., Yen, W. M., Schawlow, A. L. & White, R. M. Observation of a spin-wave sideband in the optical spectrum of MnF$_2$. *Phys. Rev. Lett.* **15**, 656–659 (1965).

51. Chen, P., Lee, N., McGill, S., Cheong, S.-W. & Musfeldt, J. L. Magnetic-field-induced color change in α-Fe$_2$O$_3$ single crystals. *Phys. Rev. B* **85**, 174413 (2012).

52. Henderson, B. & Imbusch, G. F. *Optical Spectroscopy of Inorganic Solids* (Clarendon Press, 1989).

53. Huang, K. & Rhys, A. Theory of light absorption and non-radiative transitions in *F*-centres. *Proc. R. Soc. Lond. Ser. A, Math. Phys. Sci.* **204**, 406–423 (1950).

54. Liu, Z. et al. Observation of nonreciprocal magnetophonon effect in none-ncapsulated few-layered CrI$_3$. *Sci. Adv.* **6**, eabc7628 (2020).

55. Nomura, T. et al. Phonon magnetochiral effect. *Phys. Rev. Lett.* **122**, 145901 (2019).

56. Leung, F., Chiu, W. & Demokan, M. Fiber-optic current sensor developed for power system measurement. In *1991 International Conference on Advances in Power System Control, Operation and Management, APSCOM-91*, (ed. Ross, D.). 637–643 (Institution of Engineering and Technology (IET), Hong Kong, 1991).

57. Guan, B. & Wang, S. Fiber grating laser current sensor based on magnetic force. *IEEE Photon. Technol. Lett.* **22**, 230–232 (2010).

58. Wen, F., Wu, B.-J., Li, C.-Z., Wu, S.-J. & Perumal, S. Magnetic field response of erbium-doped magneto-optic fiber Bragg grating. *Opt. Eng.* **51**, 1–5 (2012).

59. Nascimento, I. M., Baptista, J. M., Jorge, P. A. S., Cruz, J. L. & Andrés, M. V. Erbium doped optical fiber lasers for magnetic field sensing. In *24th International Conference on Optical Fibre Sensors* (eds. Kalinowski, H. J., Fabris, J. L. & Bock, W. J.) 765–768 (International Society for Optics and Photonics, SPIE, 2015).

60. Zhang, T., Zhang, J., Cheng, L., Li, Y. & Guan, B.-O. Magnetic field sensing through magnetic force using erbium-doped fiber laser. In *2017 Conference on Lasers and Electro-Optics Pacific Rim*, s1169 (Optical Society of America, 2017).

61. Kresse, G. & Hafner, J. Ab initio molecular dynamics for liquid metals. *Phys. Rev. B* **47**, 558–561 (1993).

62. Kresse, G. & Furthmüller, J. Efficient iterative schemes for ab initio total-energy calculations using a plane-wave basis set. *Phys. Rev. B* **54**, 11169–11186 (1996).

63. Dudarev, S. L., Botton, G. A., Savrasov, S. Y., Humphreys, C. J. & Sutton, A. P. Electron-energy-loss spectra and the structural stability of nickel oxide: An LSDA +U study. *Phys. Rev. B* **57**, 1505–1509 (1998).

64. Csonka, G. I. et al. Assessing the performance of recent density functionals for bulk solids. *Phys. Rev. B* **79**, 155107 (2009).

65. Blaha, P., Schwarz, K., Madsen, G. K. H., Kvasnicka, D. & Luitz, J. *WIEN2k, an Augmented Plane Wave + Local Orbitals Program for Calculating Crystal Properties* (Karlheinz Schwarz, Techn. Universität Wien, 2001).

66. Haule, K. Structural predictions for correlated electron materials using the functional dynamical mean field theory approach. *J. Phys. Soc. Jpn* **87**, 041005 (2018).

ACKNOWLEDGEMENTS

AUTHOR CONTRIBUTIONS

K.P., M.O.Y., and J.L.M. designed the study. J.Y. and S.-W.C. grew the crystals. K.P., M.O.Y., and J.L.M. discussed the measurement configurations and run pattern in detail. K.P., M.O.Y., M.G., and S.A.C. performed the pulsed-field optical measurements, and K.P. and J.L.M. analyzed the spectral data. H.-S.K., K.H., and D.V. developed a microscopic model for nonreciprocal optical effects and applied it to Ni_3TeO_6. K.P., H.-S.K., and J.L.M. wrote the manuscript. All authors commented on the text.

COMPETING INTERESTS

The authors declare no competing interests.

ADDITIONAL INFORMATION

Supplementary information The online version contains supplementary material available at https://doi.org/10.1038/s41535-022-00438-6.

Correspondence and requests for materials should be addressed to H. -S. Kim or J. L. Musfeldt.

Reprints and permission information is available at http://www.nature.com/reprints

Publisher's note Springer Nature remains neutral with regard to jurisdictional claims in published maps and institutional affiliations.